ACS OMEGA

http://pubs.acs.org/journal/acsodf

Article

Synthesis and *In Situ* Monitoring of Mechanochemical Preparation of Highly Proton Conductive Hydrogen-Bonded Metal Phosphonates

Irina Akhmetova, Max Rautenberg, Chayanika Das, Biswajit Bhattacharya,* and Franziska Emmerling*

Cite This: *ACS Omega* 2023, 8, 16687−16693

Read Online

ACCESS | Metrics & More | Article Recommendations | Supporting Information

ABSTRACT: Crystalline porous materials are recognized as promising proton conductors for the proton exchange membrane (PEM) in fuel cell technology owing to their tunable framework structure. However, it is still a challenging bulk synthesis for real-world applications of these materials. Herein, we report the mechanochemical gram-scale synthesis of two isostructural metal hydrogen-bonded organic frameworks (MHOFs) of Co(II) and Ni(II) based on 1-hydroxyethylidenediphosphonic acid ($HEDPH_4$) with 2,2′-bipyridine (2,2′-bipy): $Co(HEDPH_3)_2(2,2'\text{-bipy})\cdot H_2O$ (**1**) and $Ni(HEDPH_3)_2(2,2'\text{-bipy})\cdot H_2O$ (**2**). *In situ* monitoring of the mechanochemical synthesis using different synchrotron-based techniques revealed a one-step mechanism − the starting materials are directly converted to the product. With the existence of extensive hydrogen bonds with amphiprotic uncoordinated phosphonate hydroxyl and oxygen atoms, both frameworks exhibited proton conduction in the range of 10^{-4} S cm^{-1} at room temperature under humid conditions. This study demonstrates the potential of green mechanosynthesis for bulk material preparation of framework-based solid-state proton conductors.

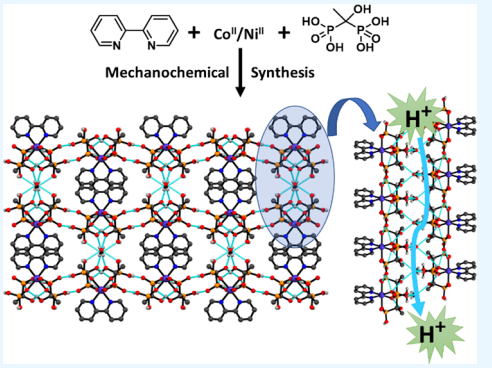

INTRODUCTION

Given the increasing environmental impact of the continuous consumption of traditional fossil fuels and the growing scarcity of these non-renewable energy sources, the development of new renewable energy sources is more urgent than ever.[1−3] In this regard, proton exchange membrane fuel cells (PEMFCs) are one of the most promising technologies that deliver high energy density without CO_2 emissions.[4,5] A solid-state proton conductor (SSPC) is the core part of PEMFCs, which directly determines the efficiency and service life of the fuel cell.[6,7] So far, Nafion and Nafion-like polymer membranes with high conductivities of 10^{-1}−10^{-2} S cm^{-1} under 60−80 °C and high relative humidity (RH) are extensively utilized as commercial proton exchange membranes (PEM).[8,9] However, their high manufacturing cost and poor performance at elevated temperatures restrict their versatility. Therefore, the development of new low-cost SSPCs with high proton conductivity under working conditions and water stability is urgently needed to make PEMFC technology a reality.

Over the last decade, scientific research on crystalline porous framework materials such as metal−organic frameworks (MOFs),[6,10,11] covalent organic frameworks (COFs),[12] and hydrogen-bonded frameworks (HOFs)[13] has attracted great interest as promising proton conductors due to their structural tunability, functionalizable porosity, and tunable channels. In addition, the high crystallinity of these materials provides the opportunity to study the proton transfer pathway and mechanism in depth and to understand the structure−function relationship.[14,15] The introduction of uncoordinated acidic and hydrophilic functional groups such as -OH, -COOH, $-SO_3H$, and $-PO_3H_2$ into the framework structure has been shown to be an efficient way to achieve superprotonic conductivity (at least 10^{-4} S cm^{-1}) by extending the hydrogen bonding with the solvent molecules in the pore of such framework materials.[14,16−18] In addition, proton-conducting guest molecules (imidazole, triazole, ammonium cations, etc.) were incorporated into the pores to increase proton conductivity.[19,20]

Recently, metal hydrogen bonded organic frameworks (MHOFs), which consist of single metal complexes stabilized by hydrogen bonds, have emerged as a new class of functional porous materials.[10,21−25] Another prominent feature is that the discrete complex has uncoordinated acidic functional groups that can be involved in the formation of a hydrogen-bonded network with guest molecules and promote proton transport. Thus, such supramolecular architectures can be selectively designed by rationally choosing the building motifs for PEMs.

Received: December 10, 2022
Accepted: February 23, 2023
Published: May 4, 2023

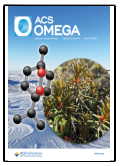

Scheme 1. Mechanochemical Synthesis of 1 and 2 by Aqueous Liquid-Assisted Grinding (LAG)

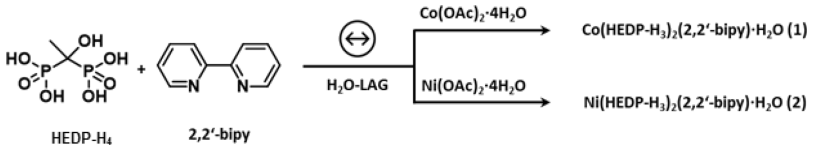

Despite the considerable level of attention these framework materials including MHOFs have gained, their synthesis still relies on the traditional solvent-based routes.[26−28] These methods are generally not cost-effective and environmentally benign. In this regard, environmentally benign rapid mechanochemical syntheses offered to address these issues for synthesizing a wide range of functional materials,[29−32] including MOFs,[33] COFs,[34] and HOFs,[35] but examples of MHOFs are scarce.

In this work, we report the mechanochemical synthesis of two isostructural MHOFs with Co(II) and Ni(II) based on 1-hydroxyethylidenediphosphonic acid with 2,2′-bipyridine as auxiliary linkers.[36] Real-time *in situ* synchrotron-based powder X-ray diffraction (PXRD) and thermography techniques have been utilized to get insights into the mechanochemical reaction pathways. Both compounds comprise well-defined hydrogen bonded network structures consisting of uncoordinated phosphonate oxygen with hydroxyl groups and lattice water molecules. Due to the simultaneous presence of a proton source (-OH) and proton acceptor (O), these MHOF materials exhibit high proton conductivity in the range of 10^{-4} S cm^{-1} at room temperature and 98% relative humidity.

RESULTS AND DISCUSSION

Two hydrogen-bonded metal phosphonate frameworks, Co$(HEDPH_3)_2$(2,2′-bipy)·H_2O (**1**) and Ni$(HEDPH_3)_2$(2,2′-bipy)·H_2O (**2**), were synthesized by an environmentally benign mechanochemical synthesis route under liquid-assisted grinding (LAG) conditions using catalytic amounts of water. Mechanochemical milling of metal acetates with 1-hydroxyethylidene-1,1-diphosphonic acid ($HEDPH_4$) monohydrate and 2,2′-bipy in the ratio 1:2:1 led to the formation of **1** or **2** (Scheme 1). Both compounds could be obtained in high yield and purity, and no side products could be detected by PXRD (Figure 1). The results of the Rietveld refinement are presented in the Supporting Information (Figure S1 and Table S1). The acquired powdery samples were washed with ethanol and air dried to remove residues of acetic acid. A detailed structural description of both compounds has already been reported as a supramolecular three-dimensional structure (Figure 2a).[36] In brief, both compounds are isostructural and metal ions are coordinated by four oxygen atoms from two different bis-chelating HEDP-H_3^- anions and two nitrogen atoms from one 2,2′-bipy ligand forming a mononuclear metal complex. The crystallographically independent molecules of the metal complex are assembled into a 2D layer via O−H···O hydrogen bonding interactions between hydroxyl groups (Figure 2b). 2D layers are further connected via hydrogen bonding interactions between lattice water molecules and phosphonate O and −OH groups in a complex fashion to form a supramolecular three-dimensional structure, which is further stabilized by $\pi-\pi$ interactions. It is worth noting that the continuous H-bonding network (Figure 2c) between the water molecules of the lattice and the uncoordinated acid phosphonate −OH groups is the key element for easy proton hopping.

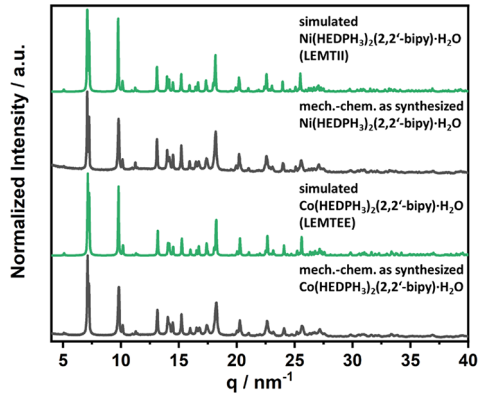

Figure 1. PXRD patterns of mechanochemically synthesized Co$(HEDPH_3)_2$(2,2′-bipy)·H_2O (**1**) and Ni$(HEDPH_3)_2$(2,2′-bipy)·H_2O (**2**) (black compared to the simulated PXRD patterns (green).

***In Situ* PXRD and Thermography of Mechanochemical Synthesis.** Mechanochemical syntheses offer a prospect to study the real-time reactions pathway by probing the phase composition and crystallinity of intermediates and products using synchrotron-based time-resolved *in situ* (TRIS) X-ray diffraction or spectroscopy.[37−39] Recently, our group has investigated the mechanochemical formation mechanism of a wide range of functional solid materials by TRIS X-ray powder diffraction, Raman spectroscopy, thermography, or combinations thereof.[40−42] However, the mechanochemical formation of metal phosphonates, especially with mixed ligands, is poorly understood. To investigate the mechanism of product formation, we monitored the mechanochemical synthesis of **1** and **2** by combined synchrotron-based TRIS PXRD and thermography techniques. During the three components grinding a loss of intensity of the diffraction signals of the starting materials was observed in the early stage of reactions. This could be ascribed to the powder getting stuck in the milling vessel or amorphization of the starting materials (Figure 3). After 30 s of milling, reflections of **1** and **2** were observed without any reflections from the starting materials (Figure 3). The crystallinity of the products was stable upon prolong milling. The corresponding temperature profiles show a steep increase in temperature with ΔT around 14.5 K (**1**) and 11 K (**2**) during the first 4 and 3 min of milling, respectively (Figure 3). The temperature rise could be attributed to the consequence of friction between the milling balls and the milling vessel. Hence, the above study clearly suggests that the mechanochemical formation of both mixed ligand MHOFs occurs via simultaneous coordination of both ligands to the metal center and not by subsequent coordination of ligands.

FT-IR and thermal gravimetric (TG) analysis of mechanochemically prepared powders of **1** and **2** also resemble the previously reported hydrothermally synthesized compounds.[36]

https://doi.org/10.1021/acsomega.2c07883
ACS Omega 2023, 8, 16687−16693

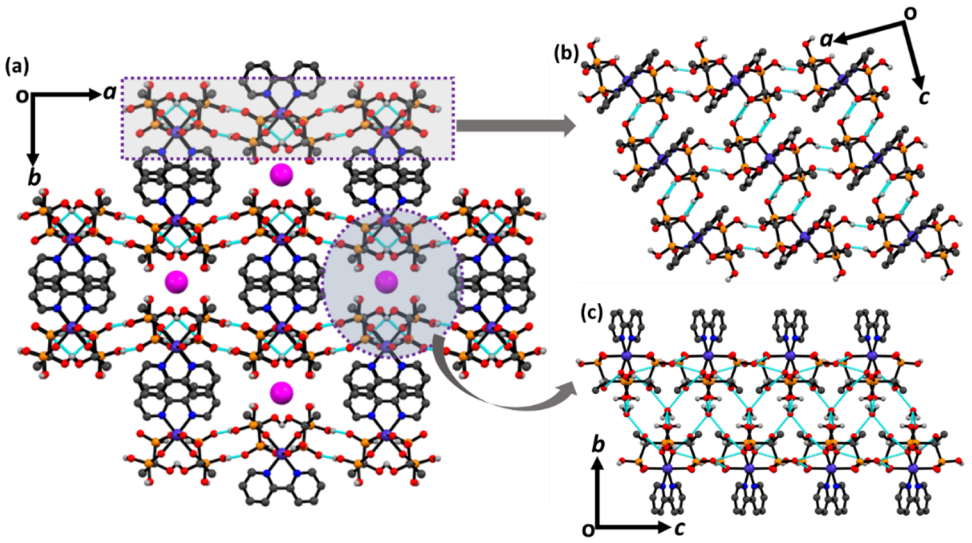

Figure 2. Crystal structure of **1** and **2**: (a) Supramolecular 3D network (magenta spheres signify the lattice water molecules and H-bonding: cyan dotted lines); (b) 2D layer hydrogen bonded network structure connected by discrete molecular complexes by an O−H···O hydrogen bond; (c) view of continuous hydrogen-bonding interaction (cyan dotted lines) between lattice water and uncoordinated acidic OH of the phosphonate groups.

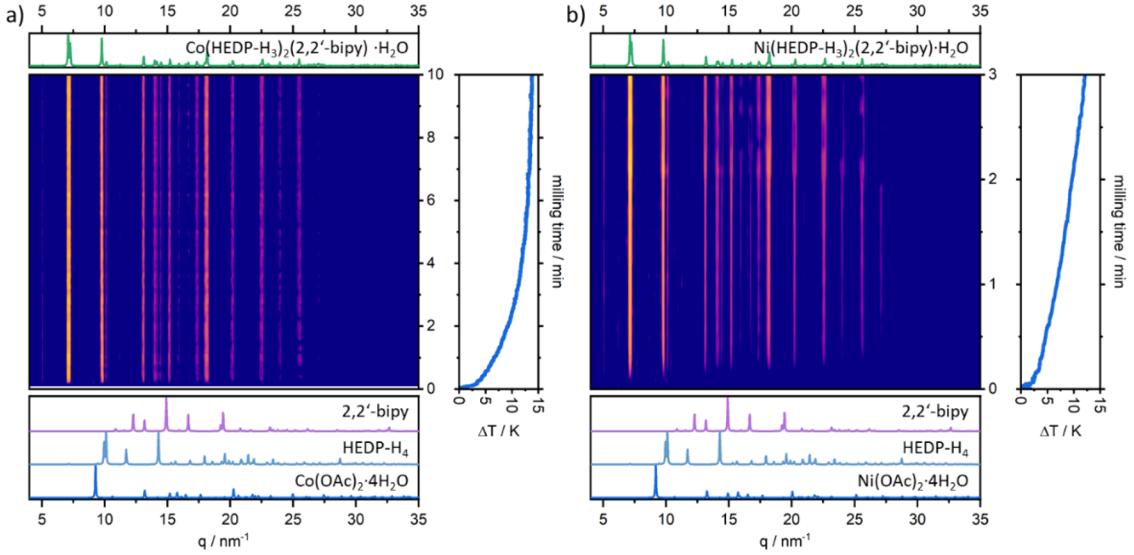

Figure 3. TRIS PXRD patterns (right) and thermography (left) of the mechanochemical formation of **1** (a) and **2** (b), respectively.

Details of FT-IR spectra are described in the Supporting Information (Figure S2). In the case of TG analysis, both compounds show a gradual mass loss of 3% of the initial mass in the temperature range of 30−180 °C, which can be attributed to the loss of lattice water molecules (calc. 2.8%). Further heating results in a gradual mass loss, which is followed by decomposition starting at 200 °C for **1** and 220 °C for **2** (Figure S3). To understand the changes of the crystal lattice, variable temperature PXRD was performed in the range of 50−210 °C. The data show no change in crystal structure upon heating of **1**, but a loss of crystallinity starting in a temperature range of 150−185 °C to amorphous material (Figure S4). Compound **2** shows structural stability up to 180 °C, and after that, crystallinity decreases. No reversible phase transformations were observed during cooling down to 25 °C for both samples (Figure S4).

To check the water affinity of **1** and **2**, dynamic vapor sorption (DVS) of water was carried out at room temperature. Hence, we have activated both compounds by heating at 170 °C for 5 h under vacuum. Both compounds exhibited similar two-step water uptake profiles and showed a final uptake of 157 cm^3/g for **1** and 146 cm^3/g for **2** at 95% RH, which correspond to uptake of 4.4 and 4 water molecules per formula unit, respectively (Figure 4). The desorption curves do not follow the sorption, showing a distinct hysteresis. The hysteresis is due to some kinetic trapping of water molecules in the small pore windows in the frameworks during desorption (Figure S5).

Proton Conductivity Measurements. The well-developed hydrogen-bonded network, temperature stability, and affinity toward water of both materials led us to explore the proton conductive properties of **1** and **2**. The proton conductivity measurements were performed over a large range of relative humidity (RH) levels (68−98%, at a constant temperature of 25 °C) and temperatures (25−90 °C, at a constant humidity of 98% RH) by alternating current (AC)

https://doi.org/10.1021/acsomega.2c07883
ACS Omega 2023, 8, 16687−16693

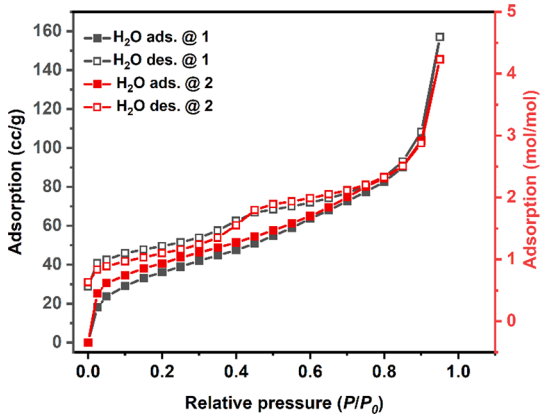

Figure 4. Water uptake of compounds **1** and **2** measured at 298 K; filled and empty symbols represent the adsorption and desorption isotherms, respectively.

electrochemical impedance spectroscopy (EIS), and the EIS results were represented in the Nyquist form (Figure 5). At first, the EIS of palletized powder samples were recorded under various RH values. The Nyquist plots of both samples showed a semicircle at the high-frequency region followed by an elongated tail at the low-frequency region except at lower RH of 68% and 73% where two semicircles were seen at the high and medium frequency region along with the low frequency tail (Figure 5a,b). The Nyquist plots for both samples from RH 78−98% were fitted to a suitable equivalent circuit ((*R*1/*Q*1) + (*R*2/*Q*2) + *Q*3), where *R*1 and *R*2 represent resistance and *Q*1, *Q*2, and *Q*3 represent constant phase elements as shown in Figure S6. On fitting, the Nyquist plots resolved into a well-fitted high frequency semicircle with lower radius and a low frequency semicircle with a higher radius, representing the resistance of the material analogous to the proton conductivity and the contact resistance respectively. The Nyquist plots of both samples at RH 68% and 73% were fitted to ((*R*1/*Q*1) + (*R*2/*Q*2) + (*R*3/*Q*3) + *Q*4), with an extra RQ in combination to account for the extra semicircle at the medium frequency region. On fitting, the plots were resolved into two well-fitted semicircles at high and medium frequency and a low frequency semicircle with a large radius. The conductivities were calculated from the fitted high frequency semicircle of the Nyquist plots and were found to be highly dependent on the relative humidity (Figure 5a,b). The samples showed very poor proton conductivity at low RH. On increasing the RH, keeping the temperature constant at 25 °C, the conductivity increased 2-fold and reached 2.4×10^{-4} and 4.2×10^{-4} S cm^{-1}, respectively for **1** and **2** at 98% RH (Figure 5a-b). As observed from the water absorption profile of both **1** and **2**, absorption of water increased as the vapor pressure increased from 60−98% (Figure 4). Thus, the increase in the proton conductivity with increasing RH is due to the formation of a well-connected network of absorbed water molecules with lattice water and H-bonds.

Proton conductivity measurements were also done at variable temperature and constant RH of 98%. The Nyquist plots of both samples showed a semicircle at the high

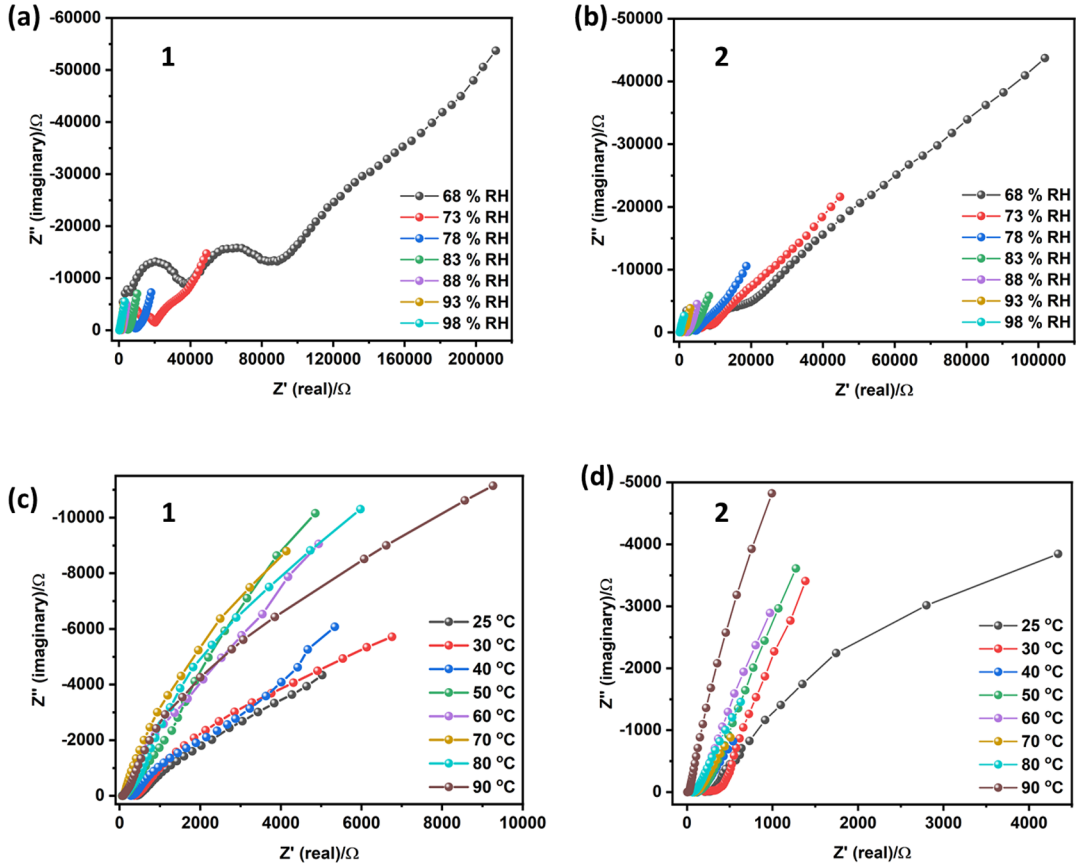

Figure 5. Nyquist plot for (a, b) **1** and **2**, respectively, at different relative humidities (RH) and 25 °C; (c, d) **1** and **2**, respectively, at different temperatures and 98% RH.

https://doi.org/10.1021/acsomega.2c07883
ACS Omega 2023, 8, 16687−16693

frequency region followed by an elongated tail at the low frequency region and fitted to ((*R*1/*Q*1) + (*R*2/*Q*2) + *Q*3) and the conductivity was calculated from the resolved high frequency semicircle (Figure 5c,d). On gradually increasing the temperature, the conductivities of **1** and **2** have been observed to increase, which is a typical proton conductivity behavior. At 90 °C and 98% RH, the conductivities of **1** and **2** reached maximum values of 8.0×10^{-4} and 2.5×10^{-3} S cm^{-1}, respectively (Figure 5c,d). Both compounds retained their crystallinity after the proton conductivity measurements (Figure S7). The very low activation energies (E_a) of 0.08 and 0.15 eV of **1** and **2**, respectively, (Figure 6) suggest a

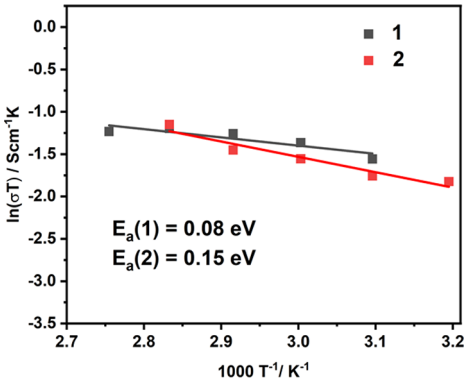

Figure 6. ln(σT) versus 1000 T^{-1}/K plots at 98% RH for **1** and **2**, respectively. The solid lines indicate the best fit of the data.

favorable transferring of protons between the H-donor and acceptor by the Grotthuss mechanism, through the well-connected H-bonded network, lattice water, and absorbed water. In the literature, very few examples of proton conductive MHOFs are reported (Table S2).[10,43] Moreover, compounds **1** and **2** are among the highest proton conducting MHOFs under high humid conditions.

CONCLUSIONS

In summary, two isostructural MHOFs, [M(HEDPH$_3$)$_2$(2,2′-bipy)]·H$_2$O (M = Co, Ni), were synthesized in the gram scale by mechanochemical synthesis. Real-time *in situ* monitoring of the synthesis by combined synchrotron-based TRIS PXRD and thermography revealed a fast and direct conversion of the starting materials to the products. Both compounds show high thermal stability and water affinity and behave as superprotonic conductors with proton conductivities of 2.4×10^{-4} and 4.2×10^{-4} S cm^{-1} at room temperature and 98% RH. The very low activation energies of 0.08 eV (for **1**) and 0.15 eV (for **2**) suggest a favorable proton transfer through the H-bonded network between uncoordinated phosphonate oxygen, hydroxyl groups with lattice water, and absorbed water molecules. This work demonstrates the potential of mechanochemical synthesis of prospective ultrahigh proton conducting MHOF materials in the bulk scale for green energy generation.

EXPERIMENTAL SECTION

General Methods. Employed chemicals were commercially acquired and used without further purification. Powder X-ray diffraction (PXRD) data were collected on a D8 Advance diffractometer (Bruker AXS, Germany). Thermogravimetric analysis (TGA) of finely ground and dried powders was performed on a heat flux TGA-DSC 3+ (Mettler-Toledo). The *in situ* PXRD measurements were performed at the μSpot beamline (BESSY II, Helmholtz Zentrum Berlin, Germany). Dynamic vapor sorption (DVS) with water vapor was carried out with a DVS resolution dual vapor gravimetric sorption analyzer (Surface Measurement Systems). *In situ* thermograms of the milling reaction were recorded with an IR camera. Proton conductivities were measured by alternative-current (AC) impedance measurements using an impedance and gain-phase analyzer (Biologic SP-150e) over a frequency range from 10 mHz to 1 MHz with an input voltage amplitude of 10 mV.

*Mechanochemical Synthesis. Co(HEDPH$_3$)$_2$(2,2′-Bipy)·H$_2$O (**1**).* In a typical mechanochemical synthesis, cobalt acetate tetrahydrate (1.172 mmol, 291.9 mg), etidronic acid monohydrate (2.344 mmol, 525.1 mg), and 2,2′-bipyridine (1.172, 183.0 mg) were added to a stainless steel milling jar (10 mL volume) together with two stainless steel milling balls (10 mm diameter, 4 g) and Milli Q water (333 μL). The mixture was ground in a Pulverisette 23 vertical ball mill at a frequency of 50 Hz for 15 min. The received damp mixture was washed with ethanol and air dried. For *in situ* PXRD experiments, a custom-made Perspex milling jar was used.

*Ni(HEDPH$_3$)$_2$(2,2′-Bipy)·H$_2$O (**2**).* Compound **2** was synthesized by a similar procedure to **1**, using Ni(OAc)$_2$·4H$_2$O (1.173 mmol; 291.4 mg) instead of Co(OAc)$_2$·4H$_2$O (1.172 mmol; 291.9 mg). A detailed description can be found in the Supporting Information.

ASSOCIATED CONTENT

Supporting Information

The Supporting Information is available free of charge at https://pubs.acs.org/doi/10.1021/acsomega.2c07883.

Experimental details; Rietveld refinement; FT-IR spectra; thermal studies; variable temperature PXRD; PXRD diffraction after water adsorption; proton conductivity (PDF)

AUTHOR INFORMATION

Corresponding Authors

Biswajit Bhattacharya − *BAM Federal Institute for Materials Research and Testing, 12489 Berlin, Germany;* orcid.org/0000-0003-4138-1287; Email: biswajit.bhattacharya@bam.de

Franziska Emmerling − *BAM Federal Institute for Materials Research and Testing, 12489 Berlin, Germany; Department of Chemistry, Humboldt-Universität zu Berlin, 12489 Berlin, Germany;* orcid.org/0000-0001-8528-0301; Email: franziska.emmerling@bam.de

Authors

Irina Akhmetova − *BAM Federal Institute for Materials Research and Testing, 12489 Berlin, Germany; Department of Chemistry, Humboldt-Universität zu Berlin, 12489 Berlin, Germany*

Max Rautenberg − *BAM Federal Institute for Materials Research and Testing, 12489 Berlin, Germany; Department of Chemistry, Humboldt-Universität zu Berlin, 12489 Berlin, Germany;* orcid.org/0000-0001-8500-1085

Chayanika Das − *BAM Federal Institute for Materials Research and Testing, 12489 Berlin, Germany*

Complete contact information is available at: https://pubs.acs.org/10.1021/acsomega.2c07883

https://doi.org/10.1021/acsomega.2c07883
ACS Omega 2023, 8, 16687−16693

Notes

The authors declare no competing financial interest.

■ ACKNOWLEDGMENTS

The authors thank Carsten Prinz for DVS experiments, "Gefördert durch die Deutsche Forschungsgemeinschaft (DFG)—Projektnummer 387284271—SFB 1349", and "Funded by the Deutsche Forschungsgemeinschaft (DFG, German Research Foundation)—Project-ID 387284271—SFB 1349".

■ REFERENCES

(1) Goldemberg, J. Ethanol for a Sustainable Energy Future. *Science* **2007**, *315*, 808−810.
(2) Chu, S.; Majumdar, A. Opportunities and Challenges for a Sustainable Energy Future. *Nature* **2012**, *488*, 294−303.
(3) Lemmon, J. P. Energy: Reimagine Fuel Cells. *Nature* **2015**, *525*, 447−449.
(4) Priya, K.; Sathishkumar, K.; Rajasekar, N. A Comprehensive Review on Parameter Estimation Techniques for Proton Exchange Membrane Fuel Cell Modelling. *Renewable Sustainable Energy Rev.* **2018**, *93*, 121−144.
(5) Firouz Tadavani, K.; Abdolmaleki, A.; Molavian, M. R.; Borandeh, S.; Sorvand, E.; Zhiani, M. Synergistic Behavior of Phosphonated and Sulfonated Groups on Proton Conductivity and Their Performance for High-Temperature Proton Exchange Membrane Fuel Cells (PEMFCs). *Energy Fuels* **2017**, *31*, 11460−11470.
(6) Lim, D.-W.; Kitagawa, H. Rational Strategies for Proton-Conductive Metal−Organic Frameworks. *Chem. Soc. Rev.* **2021**, *50*, 6349−6368.
(7) Ramaswamy, P.; Wong, N. E.; Shimizu, G. K. H. MOFs as Proton Conductors − Challenges and Opportunities. *Chem. Soc. Rev.* **2014**, *43*, 5913−5932.
(8) Mauritz, K. A.; Moore, R. B. State of Understanding of Nafion. *Chem. Rev.* **2004**, *104*, 4535−4586.
(9) Moilanen, D. E.; Spry, D. B.; Fayer, M. D. Water Dynamics and Proton Transfer in Nafion Fuel Cell Membranes. *Langmuir* **2008**, *24*, 3690−3698.
(10) Chand, S.; Pal, S. C.; Pal, A.; Ye, Y.; Lin, Q.; Zhang, Z.; Xiang, S.; Das, M. C. Metalo Hydrogen-Bonded Organic Frameworks (MHOFs) as New Class of Crystalline Materials for Protonic Conduction. *Chem. − Eur. J.* **2019**, *25*, 1691−1695.
(11) Pal, S. C.; Das, M. C. Superprotonic Conductivity of MOFs and Other Crystalline Platforms Beyond 10 $^{-1}$ S Cm $^{-1}$. *Adv. Funct. Mater.* **2021**, *31*, No. 2101584.
(12) Sasmal, H. S.; Aiyappa, H. B.; Bhange, S. N.; Karak, S.; Halder, A.; Kurungot, S.; Banerjee, R. Superprotonic Conductivity in Flexible Porous Covalent Organic Framework Membranes. *Am. Ethnol.* **2018**, *130*, 11060−11064.
(13) Karmakar, A.; Illathvalappil, R.; Anothumakkool, B.; Sen, A.; Samanta, P.; Desai, A. V.; Kurungot, S.; Ghosh, S. K. Hydrogen-Bonded Organic Frameworks (HOFs): A New Class of Porous Crystalline Proton-Conducting Materials. *Angew. Chem., Int. Ed.* **2016**, *55*, 10667−10671.
(14) Chen, J.; Mei, Q.; Chen, Y.; Marsh, C.; An, B.; Han, X.; Silverwood, I. P.; Li, M.; Cheng, Y.; He, M.; Chen, X.; Li, W.; Kippax-Jones, M.; Crawshaw, D.; Frogley, M. D.; Day, S. J.; García-Sakai, V.; Manuel, P.; Ramirez-Cuesta, A. J.; Yang, S.; Schröder, M. Highly Efficient Proton Conduction in the Metal−Organic Framework Material MFM-300(Cr)·SO $_4$ (H $_3$ O) $_2$. *J. Am. Chem. Soc.* **2022**, *144*, 11969−11974.
(15) Kolokolov, D. I.; Lim, D.; Kitagawa, H. Characterization of Proton Dynamics for the Understanding of Conduction Mechanism in Proton Conductive Metal-Organic Frameworks. *Chem. Rec.* **2020**, *20*, 1297−1313.
(16) Nagarkar, S. S.; Unni, S. M.; Sharma, A.; Kurungot, S.; Ghosh, S. K. Two-in-One: Inherent Anhydrous and Water-Assisted High Proton Conduction in a 3D Metal-Organic Framework. *Angew. Chem., Int. Ed.* **2014**, *53*, 2638−2642.
(17) Rought, P.; Marsh, C.; Pili, S.; Silverwood, I. P.; Sakai, V. G.; Li, M.; Brown, M. S.; Argent, S. P.; Vitorica-Yrezabal, I.; Whitehead, G.; Warren, M. R.; Yang, S.; Schröder, M. Modulating Proton Diffusion and Conductivity in Metal−Organic Frameworks by Incorporation of Accessible Free Carboxylic Acid Groups. *Chem. Sci.* **2019**, *10*, 1492−1499.
(18) Maity, D. K.; Otake, K.; Ghosh, S.; Kitagawa, H.; Ghoshal, D. Sulfonic Group Functionalized Mixed Ligand Coordination Polymers: Synthesis, Characterization, Water Sorption, and Proton Conduction Studies. *Inorg. Chem.* **2017**, *56*, 1581−1590.
(19) Biradha, K.; Goswami, A.; Moi, R.; Saha, S. Metal−Organic Frameworks as Proton Conductors: Strategies for Improved Proton Conductivity. *Dalton Trans.* **2021**, *50*, 10655−10673.
(20) Li, A.-L.; Gao, Q.; Xu, J.; Bu, X.-H. Proton-Conductive Metal-Organic Frameworks: Recent Advances and Perspectives. *Coord. Chem. Rev.* **2017**, *344*, 54−82.
(21) Zhu, Z.-H.; Wang, H.-L.; Zou, H.-H.; Liang, F.-P. Metal Hydrogen-Bonded Organic Frameworks: Structure and Performance. *Dalton Trans.* **2020**, *49*, 10708−10723.
(22) Qin, Y.; Wang, X.; Xie, W.; Li, Z.; Li, G. Structural Effect on Proton Conduction in Two Highly Stable Disubstituted Ferrocenyl Carboxylate Frameworks. *Inorg. Chem.* **2020**, *59*, 10243−10252.
(23) Zhai, Q.-G.; Mao, C.; Zhao, X.; Lin, Q.; Bu, F.; Chen, X.; Bu, X.; Feng, P. Cooperative Crystallization of Heterometallic Indium-Chromium Metal-Organic Polyhedra and Their Fast Proton Conductivity. *Am. Ethnol.* **2015**, *127*, 7997−8001.
(24) Garai, A.; Kumar, A. G.; Banerjee, S.; Biradha, K. Proton-Conducting Hydrogen-Bonded 3D Frameworks of Imidazo-Pyridine-Based Coordination Complexes Containing Naphthalene Disulfonates in Rhomboid Channels. *Chem. − Asian J.* **2019**, *14*, 4389−4394.
(25) Wang, H.-L.; Ma, X.-F.; Zhu, Z.-H.; Zhang, Y.-Q.; Zou, H.-H.; Liang, F.-P. A Series of Dysprosium-Based Hydrogen-Bonded Organic Frameworks (Dy−HOFs): Thermally Triggered off → on Conversion of a Single-Ion Magnet. *Inorg. Chem. Front.* **2019**, *6*, 2906−2913.
(26) Stock, N.; Biswas, S. Synthesis of Metal-Organic Frameworks (MOFs): Routes to Various MOF Topologies, Morphologies, and Composites. *Chem. Rev.* **2012**, *112*, 933−969.
(27) Geng, K.; He, T.; Liu, R.; Dalapati, S.; Tan, K. T.; Li, Z.; Tao, S.; Gong, Y.; Jiang, Q.; Jiang, D. Covalent Organic Frameworks: Design, Synthesis, and Functions. *Chem. Rev.* **2020**, *120*, 8814−8933.
(28) Lin, R.-B.; He, Y.; Li, P.; Wang, H.; Zhou, W.; Chen, B. Multifunctional Porous Hydrogen-Bonded Organic Framework Materials. *Chem. Soc. Rev.* **2019**, *48*, 1362−1389.
(29) Feiler, T.; Bhattacharya, B.; A. L. Michalchuk, A.; Schröder, V.; List-Kratochvil, E.; Emmerling, F. Mechanochemical Syntheses of Isostructural Luminescent Cocrystals of 9-Anthracenecarboxylic Acid with Two Dipyridines Coformers. *Crystals* **2020**, *10*, 889.
(30) Beillard, A.; Bantreil, X.; Métro, T.-X.; Martinez, J.; Lamaty, F. Mechanochemistry for Facilitated Access to N,N-Diaryl NHC Metal Complexes. *New J. Chem.* **2017**, *41*, 1057−1063.
(31) Bůžek, D.; Ondrušová, S.; Hynek, J.; Kovář, P.; Lang, K.; Rohlíček, J.; Demel, J. Robust Aluminum and Iron Phosphinate Metal−Organic Frameworks for Efficient Removal of Bisphenol A. *Inorg. Chem.* **2020**, *59*, 5538−5545.
(32) Guerri, A.; Taddei, M.; Bataille, T.; Moneti, S.; Boulon, M.-E.; Sangregorio, C.; Costantino, F.; Ienco, A. Same Not the Same: Thermally Driven Transformation of Nickel Phosphinate-Bipyridine One-Dimensional Chains into Three-Dimensional Coordination Polymers. *Cryst. Growth Des.* **2018**, *18*, 2234−2242.
(33) Rautenberg, M.; Bhattacharya, B.; Das, C.; Emmerling, F. Mechanochemical Synthesis of Phosphonate-Based Proton Conducting Metal−Organic Frameworks. *Inorg. Chem.* **2022**, *61*, 10801−10809.
(34) Shinde, D. B.; Aiyappa, H. B.; Bhadra, M.; Biswal, B. P.; Wadge, P.; Kandambeth, S.; Garai, B.; Kundu, T.; Kurungot, S.; Banerjee, R. A Mechanochemically Synthesized Covalent Organic Framework as a

https://doi.org/10.1021/acsomega.2c07883
ACS Omega 2023, 8, 16687−16693

Proton-Conducting Solid Electrolyte. *J. Mater. Chem. A* **2016**, *4*, 2682−2690.
(35) Qin, W.; Si, D.; Yin, Q.; Gao, X.; Huang, Q.; Feng, Y.; Xie, L.; Zhang, S.; Huang, X.; Liu, T.; Cao, R. Reticular Synthesis of Hydrogen-Bonded Organic Frameworks and Their Derivatives via Mechanochemistry. *Angew. Chem., Int. Ed.* **2022**, *61*, No. e202202089.
(36) Zheng, M.-J.; Zhu, Y.-Y.; Sun, Z.-G.; Zhu, J.; Jiao, C.-Q.; Chu, W.; Sun, S.-H.; Tian, H. Synthesis, Crystal Structures, and Surface Photovoltage Properties of Four New Metal Diphosphonates Based on the Mixed Ligands. *CrystEngComm* **2013**, *15*, 1445.
(37) Friščić, T.; Halasz, I.; Beldon, P. J.; Belenguer, A. M.; Adams, F.; Kimber, S. A. J.; Honkimäki, V.; Dinnebier, R. E. Real-Time and in Situ Monitoring of Mechanochemical Milling Reactions. *Nat. Chem.* **2013**, *5*, 66−73.
(38) Lukin, S.; Užarević, K.; Halasz, I. Raman Spectroscopy for Real-Time and in Situ Monitoring of Mechanochemical Milling Reactions. *Nat. Protoc.* **2021**, *16*, 3492−3521.
(39) Germann, L. S.; Katsenis, A. D.; Huskić, I.; Julien, P. A.; Užarević, K.; Etter, M.; Farha, O. K.; Friščić, T.; Dinnebier, R. E. Real-Time in Situ Monitoring of Particle and Structure Evolution in the Mechanochemical Synthesis of UiO-66 Metal−Organic Frameworks. *Cryst. Growth Des.* **2020**, *20*, 49−54.
(40) Kulla, H.; Haferkamp, S.; Akhmetova, I.; Röllig, M.; Maierhofer, C.; Rademann, K.; Emmerling, F. In Situ Investigations of Mechanochemical One-Pot Syntheses. *Angew. Chem., Int. Ed.* **2018**, *57*, 5930−5933.
(41) Kulla, H.; Wilke, M.; Fischer, F.; Röllig, M.; Maierhofer, C.; Emmerling, F. Warming up for Mechanosynthesis − Temperature Development in Ball Mills during Synthesis. *Chem. Commun.* **2017**, *53*, 1664−1667.
(42) Michalchuk, A. A. L.; Emmerling, F. Time-Resolved In Situ Monitoring of Mechanochemical Reactions. *Angew. Chem., Int. Ed.* **2022**, No. e202117270.
(43) Shi, Z.-Q.; Ji, N.-N.; Guo, K.-M.; Li, G. Crystalline Hydrogen-Bonded Supramolecular Frameworks (HSFs) as New Class of Proton Conductive Materials. *Appl. Surf. Sci.* **2020**, *504*, No. 144484.

https://doi.org/10.1021/acsomega.2c07883
ACS Omega 2023, 8, 16687−16693